

Characterization and Reduction Roasting Studies of an Iron Rich Manganese Ore

Swagat S. Rath¹ · Sunil Kumar Tripathy² · Danda S. Rao¹ · Surendra K. Biswal¹

Received: 9 March 2017 / Accepted: 20 October 2017 / Published online: 4 November 2017
© The Indian Institute of Metals - IIM 2017

Abstract The article presents the reduction roasting followed by low intensity magnetic separation studies of a low grade Mn ore assaying 27.7% Mn and 26.1% Fe in order to obtain a Mn rich non-magnetic concentrate. The reflected light microscopic studies followed by the liberation studies of the as-received sample using quantitative mineralogical evaluation by scanning electron microscope suggested a poor liberation pattern of the constituent Mn and Fe minerals owing to a complex association of the different phases present. The reduction roasting studies carried out while varying different process parameters such as ore particle size, temperature, reductant content and residence time ended up with products containing 45–48% Mn with a Mn/Fe ratio of 5–6 at a yield of ~ 60% with the optimum level of conditions such as temperature: 800–850 °C, time: 90–120 min and charcoal: 10–12%. The scanning electron microscopy–energy dispersive X-ray spectroscopy studies of the roasted product reported manganoite as the major Mn bearing phase while magnetite was found to be the major iron bearing phase.

Keywords Reduction roasting · QEMSCAN · Mn to Fe ratio · SEM–EDS · Reflected light microscopy

1 Introduction

Manganese ore is a useful raw material for the steel, chemical, paint, fertilizer and battery industries. In India, more than 90% of the manganese ores are consumed by the iron and steel industry in the form of different ferroalloys [1, 2]. There is an increasing demand for manganese ore, greatly due to the increase in the manufacture of steel over the years and the diminishing natural resources [3]. Therefore, the utilization and exploitation of low-grade manganese ores have become very important. In addition, enormous quantities of low-grade fines are generated during mining, beneficiation, and handling of different ore deposits, which contain Fe, Al, Si, P, S as the gangue components in different mineral phases. India, with 142 million tons of manganese deposits ranks fifth in the world. Indian manganese ore occurs mainly as syngenetic sedimentary bedded deposits as well as secondary supergene epigenetic deposits [4]. Odisha state contributes about 30% of the total manganese ore deposit in India, and the ore deposit is mostly ferruginous as well as friable in nature [5]. Moreover, the generation of large quantities of low-grade manganese ore fines have resulted in the accumulation of large amounts of inferior-quality ore being dumped at the mine sites, resulting in acute space constraints and environmental hazards [6, 7]. So, the utilization of these low-grade deposits happens to be a major challenge for the manganese ore mining and mineral industries.

The Mn/Fe ratio in manganese ores is a critical factor in the ferroalloy industries. A major consumption of the manganese in the steel industry is in the form of ferro-manganese which needs manganese ore having a Mn/Fe ratio higher than 5 so as to facilitate its operation in the submerged arc furnace. Usually, the low-grade manganese ores are beneficiated using the gravity separation methods

✉ Danda S. Rao
dsrao@immet.res.in

¹ CSIR-Institute of Minerals and Materials Technology, Bhubaneswar, India

² Tata Steel Limited, Jamshedpur, India

by exploiting the density difference between the associated minerals. Similarly, magnetic separation (based on the magnetic susceptibility) and flotation (based on the surface property) are also used for up-gradation. The efficiency of the separation decreases when the gangue minerals are of similar density or magnetic susceptibility as that of the manganese ore minerals. Reduction roasting followed by magnetic separation to separate iron bearing gangue minerals is also a pre-treatment method reported in the literature. There are a few publications available on this particular research topic, and a brief summary of the review is mentioned here.

Gravity separation studies for manganese ore are mostly aimed at the removal of silicate, alumina, P and S from the low/subgrade deposits. The studies like washing, jigging, tabling, teeter bed separation, etc. are employed to upgrade the siliceous or alumina bearing low-grade manganese fines [8–16]. However, most of these studies were restricted to siliceous ore deposits. In general, the complexity of these separations is directly related to the liberation pattern of the manganese-bearing minerals and the associated gangue constituents [17]. However, the process route using gravity separation is not efficient when the iron-bearing minerals occur as the major gangue components. Similarly, several flotation studies have been carried out on these kind of ores [18–20]. Dry and wet magnetic separation studies have been carried out for different low-grade deposits by using induced roll magnetic separator, permanent roll magnetic separator, rare earth rolls magnetic separator, rare earth drum magnetic separator and wet high-intensity magnetic separator [21–26]. Dry separation is normally employed for upgrading the coarser particle size fractions, whereas fine/ultrafine fractions are concentrated using wet high-intensity magnetic separation. However, the separation of the iron bearing gangue minerals does not adequately get separated due to the presence of near magnetic susceptibility particles in the sample. In this context, the enrichment of the manganese content and the Mn/Fe ratio of a complex manganese ore from the Nishikhal deposit, India, containing 32% Mn, 18% Fe, 16% SiO₂, 21% acid-insoluble components, and 0.45% phosphorous has been studied. Using the approach of reduction roasting followed by magnetic separation, the Mn content of the product can be enriched to 40% with the Mn/Fe ratio increased to 10 and the phosphorous content decreased to 0.3% [27]. Similar studies have also been conducted on Indian manganese deposits to improve the manganese-to-iron ratio of the product through optimization of the reduction roasting process followed by magnetic separation [28, 29]. However, all these studies have not been focussed much on understanding the roasting process, and its influence on the manganese-to-iron ratio of the low grade manganese ore, due to limited experimentation.

Most of the literatures published on low-grade manganese ore deposits have been limited to the siliceous-type ores (dominated by silicate-bearing gangue minerals), for which WHIMS has predominantly been used for upgrading at finer sizes whereas gravity separation studies for the coarser particle size range. However, the literature contains very few studies on the reduction roasting followed by magnetic separation for ferruginous manganese ores, except for a few attempts on the feasibility of the process. Taking into consideration all these facts and figures as discussed above, the present work attempts the reduction roasting-magnetic separation studies of a low grade iron rich manganese ore. Different process parameters have been varied while a detailed characterisation of the feed and some of the roasted products have been carried out in order to understand the formation of different phases during the roasting process.

2 Materials and Methods

2.1 Sample Details

The iron rich manganese ore used in the present work was collected from the mines of Joda area in the Odisha State of India. The samples were mixed thoroughly and crushed to below 10 mm size. The chemical analysis of the sample indicated the presence of 27.7% Mn, 26.1% Fe, 10.6% SiO₂, 5.6% Al₂O₃, 8.9% loss on ignition (LOI), 0.069% P and 0.004% S. The Mn to Fe ratio was found to be 1.06. The sample was found to have a bulk density of 2.224 g/cc, a specific gravity of 3.5 and moisture content of 0.44%. The angle of repose of the crushed sample was calculated to be 38.3° while the porosity (determined using a Quantachrome make gas sorption analyzer) and Bond's work index were 36.45% and 14.1 kWh/tonne respectively. Activated charcoal containing 93.5% fixed carbon (FC), 2.5% ash, 1.0% volatile matter, and 3.0% moisture was used as the reductant.

2.2 Reduction Roasting and Magnetic Separation

All the reduction roasting experiments were conducted in a laboratory muffle furnace. For each roasting experiment, 200 g of the manganese fines along with the desired amount of activated charcoal was thoroughly mixed, put in a refractory crucible and placed inside the furnace set at the desired temperature. The sample after being roasted for a pre-determined time was taken out and immediately quenched with water in order to prevent oxidation of the reduced products. The roasted mass was ground to below 75 μm size so as to allow maximum liberation of the mineral phases and then subjected to low intensity

magnetic separator (LIMS) at a magnetic intensity of ~ 1800 G. The magnetic and nonmagnetic fraction were collected separately, dried, and analyzed for Mn and Fe content. The non-magnetic fraction was regarded as the product.

2.3 Characterization Techniques

Different integrated instrumental characterization studies were carried out for the feed sample and some of the roasted products. The studies of mineral liberation and modal analysis were carried out using QEMSCAN. A representative sample of the feed Mn ore was crushed to a particle size below 1 mm, wet sieved into six different size fractions, and the polished sections of each size were prepared by conventional methods. Graphite powder was used to de-agglomerate the particles. Each polished section was scanned under QEMSCAN for the modal analysis as well as liberation pattern of Mn and Fe bearing particles in each size fraction. Optical microscopic studies were carried out using a Leitz make instrument while the SEM–EDS studies were conducted using the Zeiss SEM equipped with a Bruker EDS detector.

3 Results and Discussion

3.1 Feed Characterization

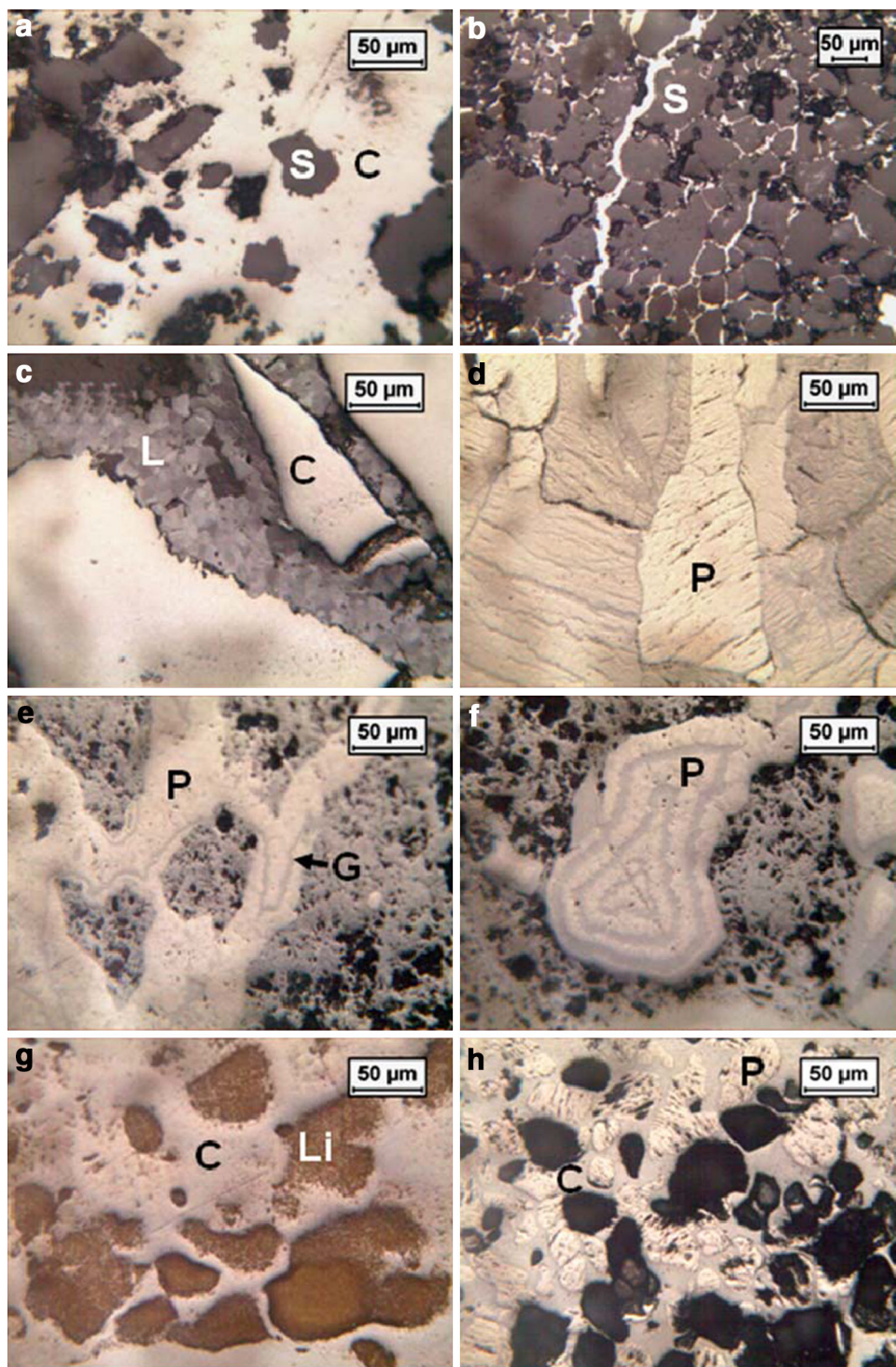
The hand specimen examination shows that the ore varies widely in its physical look as well as in its nature. The specimens reveal that the samples vary from being very hard as well as siliceous to soft friable and rich in clayey material. Considering the wide variety of hand specimens, a number of polished sections were prepared and studied under reflected light microscopes. The optical micrographs as displayed in Fig. 1 indicate that the grain sizes for various types of phases like silicates, and manganese oxide phases, vary widely as well as unevenly, from coarse to fine (Fig. 1a, b) and the intergrowth between the constituent minerals is very complex and complicated. Cryptomelane can be seen along the grain boundaries of the silicate minerals. Lithiophorite occurs as fine fibrous as well as granules along with pyrolusite and in association with the clay materials (Fig. 1c). In the majority of the cases, the pyrolusite crystals are found to be coarse grained and various shapes and sizes of it are enclosed within the matrix of cryptomelane as well as clay (Fig. 1d). It is also observed that alternate layers of cryptomelane and pyrolusite are enclosed in a matrix of goethite. In some cases, the veins of pyrolusite are found to be enclosing goethite and vice versa (Fig. 1e, f). Other than hematite and goethite, the sample also contains limonite as another iron

bearing phase. Fibrous cryptomelane is present within the clayey material and colloform bands of goethite (Fig. 1g, h). In general, it can be concluded that quartz and clay are the silicate minerals; hematite, goethite and limonite are the iron phase minerals in the sample interlocked with the manganese phases like pyrolusite, cryptomelane, psilomelane and lithiophorite in a complex manner. From the microscopic studies as discussed above, it can be predicted that the liberation of iron phases from the sample is difficult by physical beneficiation and the ratio of Mn/Fe cannot be improved significantly. The ore mineralogy along with the silica and iron contents in the present sample is more or less similar to the Nishikhal Mn ores of Odisha reported by Acharya et al. [28, 29]. However, they reported their sample to be of high phosphorous content. The phosphorous was found to be present in the form of apatite mineral, colophane as well as in an adsorbed state with pyrolusite, cryptomelane and goethite. However, the present sample does not have any significant phosphorous content.

The feed sample was also subjected to SEM–EDS studies and the results are displayed in Fig. 2 and the corresponding EDS results are given in Table 1. The sample shows the presence of goethite in many forms such as nodular and colloform, and at times as patches. Goethite and pyrolusite are found to be in close association with kaolinite (Fig. 2a, b). Lithiophorite is found as fine grained patches as well as within fine grained cryptomelane (Fig. 2c). Traces of zircon are observed within cryptomelane in the sample (Fig. 2d). The SEM–EDS studies infer that the mineral phases are associated in a very complex manner. The EDS data in Table 1 reveal significant amounts of Co in goethite and Ni in lithiophorite. The Mn mineral lithiophorite has been identified by the presence of significant amount of Al with Mn.

All the iron oxide particles and manganese minerals were considered as a single phase of iron oxide and manganese oxide phase respectively for the QEMSCAN studies. This consideration was undertaken because the QEMSCAN library does not have lithiophorite and limonite. All other oxides, sulphates and silicates (quartz, kaolinite, Mn silicate, and muscovite) were considered as individual systems of mineral phases for the estimation of the quantitative mineralogical data. However, for the estimation of the liberation data of all the silicates as mentioned above were considered as one system. The quantitative mineralogical data shown in Table 2 reveal that the iron oxide phases (hematite, goethite and limonite) are highest in abundance (39.71%) followed by the manganese oxide (38.78%) minerals (pyrolusite, cryptomelane and lithiophorite). Manganese silicates (garnets) constitute the highest (10.46%) among silicates followed by quartz (5.96%). Minor amounts of muscovite, kaolinite and traces of ilmenite and barite are also reported

Fig. 1 Reflected light photomicrographs showing feed ore, **a** Islands of silicate (*S*) minerals within cryptomelane (*C*), **b** cryptomelane (white) along the grain boundaries of the silicate minerals, **c** lithiophorite (*L*) enclosing as well as enclosed by cryptomelane (*C*), **d** very thin laths/veins of cryptomelane within coarse grained pyrolusite (*P*), **e** pyrolusite (*P*) enclosing goethite laths (shown by arrow) as well as enclosed by goethite (*G*), **f** Alternate layers of goethite and pyrolusite (*P*) and pyrolusite in turn surrounded by goethite matrix, **g** cryptomelane (*C*) contains islands of limonite (*Li*), **h** crystals of pyrolusite (*P*) and cryptomelane (*C*) interlocked very complexly and complicatedly. The black spots are the spot clay materials which are removed during polishing



by QEMSCAN in this sample. The liberation data shown in Table 2 suggest that 25.02% out of the 38.78% Mn minerals are liberated completely while 15.53% of the 39.71% iron oxide phases are liberated. Further, the data indicate that the degree of liberation of Mn and Fe minerals goes on increasing with a decrease in the particle size till the size fraction $-75 + 38 \mu\text{m}$. However, in case of the $-38 \mu\text{m}$

size fraction, the degree of liberation is lesser compared to the $-75 + 38 \mu\text{m}$ size fraction. This may be attributed to the complex interlocking textures such as colloform and banding, extremely fine grain size of lithiophorite as well as cryptomelane, and inclusions of iron and silicate minerals in Mn minerals and vice versa at this size fraction. Further, these liberation data elucidate that physical

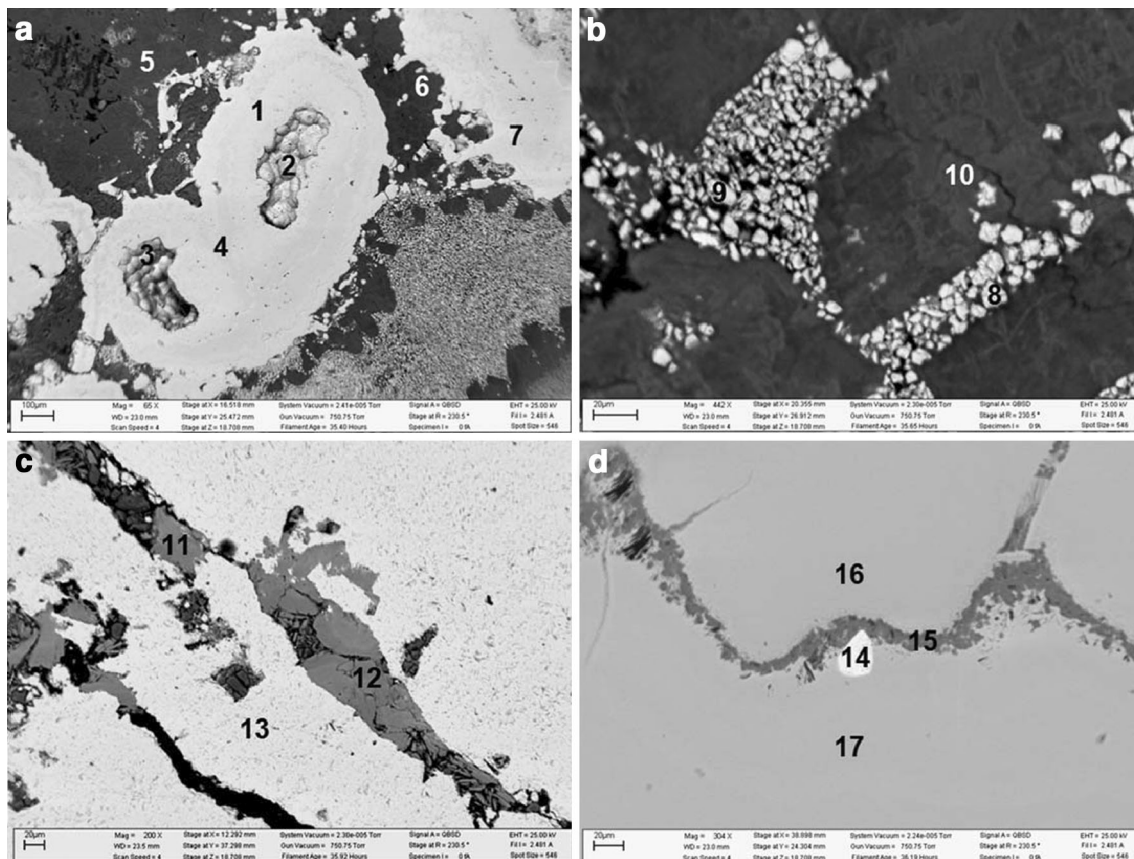


Fig. 2 SEM BSE images of the feed sample showing, **a** various forms of goethite (nodular as in point nos. 2 and 3; patches as in point no. 7 and colloform as in point nos. 1 and 4) in close association with kaolinite (point nos. 4 and 5), **b** granular pyrolusite as point no. 7 and 8 and within kaolinite patches as in point no. 10, **c** patches of lithiophorite as in point nos. 11 and 12 within the fine grained cryptomelane as point no. 13, **d** fine grained zircon as point no. 14 enclosed within cryptomelane (16, 17). A vein of lithiophorite (15) is enclosed within cryptomelane

beneficiation may not practically lead to a satisfactory separation of the Fe and Mn minerals present in the ore.

3.2 Roasting Studies

3.2.1 Effect of Particle Size and Temperature

Initially, the roasting experiments were carried out with particle sizes and temperature as the variables. The feed sample was reduced to six different particles such as – 10, – 5, – 3, – 1, – 0.5 and – 0.25 mm and each of the size fractions were subjected to four different levels of temperatures such as 600, 700, 800 and 900 °C. The other variables such as reduction time and reductant percentage were kept fixed at 120 min and 10% respectively. The results of the effect of temperature at different particle sizes are given in Fig. 3.

It is observed that as the temperature increases, there is a decrease in the yield to the non-magnetic fraction up to 800 °C and thereafter it increases (Fig. 3a). The Mn

content along with the Mn to Fe ratio of the non-magnetic fraction is maximum at 800 °C (Fig. 3b, c). This may be due to the conversion of the majority of the iron oxide phases to magnetite at 800 °C, that ultimately reports in the magnetic fraction of the LIMS thereby enhancing the non-magnetic yield and increasing the Mn to Fe ratio in the magnetic fraction. It is found that reduction is more effective for the finer size fractions compared to the coarser sizes. As the particle size decreases, the reduction from hematite to magnetite gets enhanced as evident from the high non-magnetic yield accompanied by a relatively lower Mn grade obtained in the case of the particle size of – 10 mm. However, the yield in the case of – 0.25 mm particle size (52.6%) is slightly higher compared to that of – 0.5 mm (50.5%), which is against the trend. This may be attributed to the over reduction of the iron oxide phases and transformation to wustite leading to a higher non-magnetic yield. It may be noted that wustite is a feebly magnetic product and reports in the non-magnetic fraction when separated by a low intensity magnetic separator.

Table 1 SEM–EDS semi-quantitative mineral chemistry of various mineral phases of the feed sample with the numbers 1–17 corresponding to the points marked in the photo-micrographs shown in Fig. 2

Elements	1	2	3	4	5	6	7	8	9	10	11	12	13	14	15	16	17
	Mineral																
	G	G	G	G	K	K	G	P	P	K	L	L	H	Z	L	C	C
O	41.2	41.1	46	41.7	62.9	61.3	38.9	34.1	38.8	61.4	38.6	40.3	30.3	28.5	43.6	36	39.5
Fe	54.9	55.7	49.1	54.6	0.09	0.46	57.1	1.01	1.04	0.1	1.37	1.42	66.2	0.31	1.6	0.78	0.65
Mg	0.03	0.01	0.18	0.02	0.11	ND	0.04	ND	ND	ND	0.07	0.09	0.06	ND	0.14	ND	ND
Al	0.47	0.16	1.35	0.51	21	21.4	1.32	0.24	0.2	21.7	13.5	13.8	1.12	0.48	12	0.29	0.2
Si	0.29	0.31	0.58	0.33	15.6	16.6	0.37	ND	0.04	16.2	ND	ND	ND	11.7	0.2	ND	ND
P	0.27	0.15	0.34	0.28	ND	ND	0.1	0.18	0.1	ND	ND	ND	ND	ND	ND	ND	ND
Mn	0.81	0.66	0.84	0.69	0.01	ND	0.49	63.8	58.9	0.33	42.8	42.7	0.6	1.67	37	59.2	57.2
Co	1.12	1.12	0.95	1.03	ND	ND	0.96	ND	ND	ND	0.19	0.21	1.04	ND	0.35	0.04	ND
Ni	0.18	0.07	0.08	0.16	0.04	0.02	0.18	0.05	0.08	0.06	1.41	0.27	0.04	0.24	3.01	0.04	0.02
Cu	0.23	0.24	0.15	0.22	0.07	0.07	0.14	0.09	0.19	0.1	1.19	0.72	0.19	ND	ND	0.22	0.13
Zn	0.53	0.56	0.45	0.44	0.13	0.11	0.47	0.34	0.49	0.17	0.81	0.49	0.44	0.32	0.52	0.45	0.28
Ba	ND	ND	ND	ND	0.02	0.04	ND	0.05	ND	ND	0.06	ND	0.1	ND	0.1	0.4	0.07
Ca	ND	ND	ND	ND	ND	ND	ND	ND	ND	ND	ND	ND	ND	0.08	ND	ND	0.02
Sc	ND	ND	ND	ND	ND	ND	ND	ND	ND	ND	ND	ND	ND	0.33	ND	ND	ND
K	ND	ND	ND	ND	ND	ND	ND	ND	ND	ND	ND	ND	ND	ND	0.27	2.44	1.93
Ti	ND	ND	ND	ND	ND	ND	ND	ND	ND	ND	ND	ND	ND	ND	0.15	ND	ND
Cr	ND	ND	ND	ND	ND	ND	ND	ND	ND	ND	ND	ND	ND	ND	0.03	0.09	0.07
Zr	ND	ND	ND	ND	ND	ND	ND	ND	ND	ND	ND	ND	ND	53.7	ND	ND	ND
Hf	ND	ND	ND	ND	ND	ND	ND	ND	ND	ND	ND	ND	ND	2.67	ND	ND	ND

All the values are given in wt%

G goethite, K kaolinite, P pyrolusite, L lithiophorite, H hematite, Z zircon, C cryptomelane, ND not detected

Table 2 Quantitative mineralogy and degree of liberation as determined by QEMSCAN

Phases	Size fraction (μm)						Combined
	– 1000 + 500	– 500 + 250	– 250 + 125	– 125 + 75	– 175 + 38	– 38	
<i>(a) Quantitative Mineralogy for various different phases</i>							
Muscovite	0.46	0.26	0.19	0.07	0.1	1.17	2.24
Quartz	1.09	0.77	0.91	0.46	0.63	2.1	5.96
Kaolinite	0.62	0.26	0.25	0.11	0.16	1.19	2.6
Mn–silicate	0.48	0.29	0.18	0.09	0.09	9.33	10.46
Ilmenite	0.01	0.01	0.02	0.01	0.03	0.08	0.15
Barite	0.03	0.01	0.01	0	0.01	0.06	0.11
Mn Minerals	14.34	7.61	4.59	2.51	2.55	7.18	38.78
Fe Minerals	15.66	8.61	4.85	2.95	3.24	4.4	39.71
<i>(b) Degree of liberation in different size fraction (%)</i>							
Mn minerals	9.41	29.79	38.73	52.95	64.33	18.66	25.02
Fe minerals	4.15	13.01	19.58	36.77	53.54	14.25	15.53
Silicate minerals	9.20	29.46	46.03	55.74	67.55	28.40	30.08

All the values are given in wt%

The Mn content in the non-magnetic fraction is around 41–42% for the particle sizes of – 3 mm, – 1 mm, – 500 μm and – 250 μm while the Mn/Fe ratio of 7.9 is

the highest obtained in case of the size fraction of – 250 μm . This may again be attributed to the larger surface area in case of the fine size fractions. Also, the

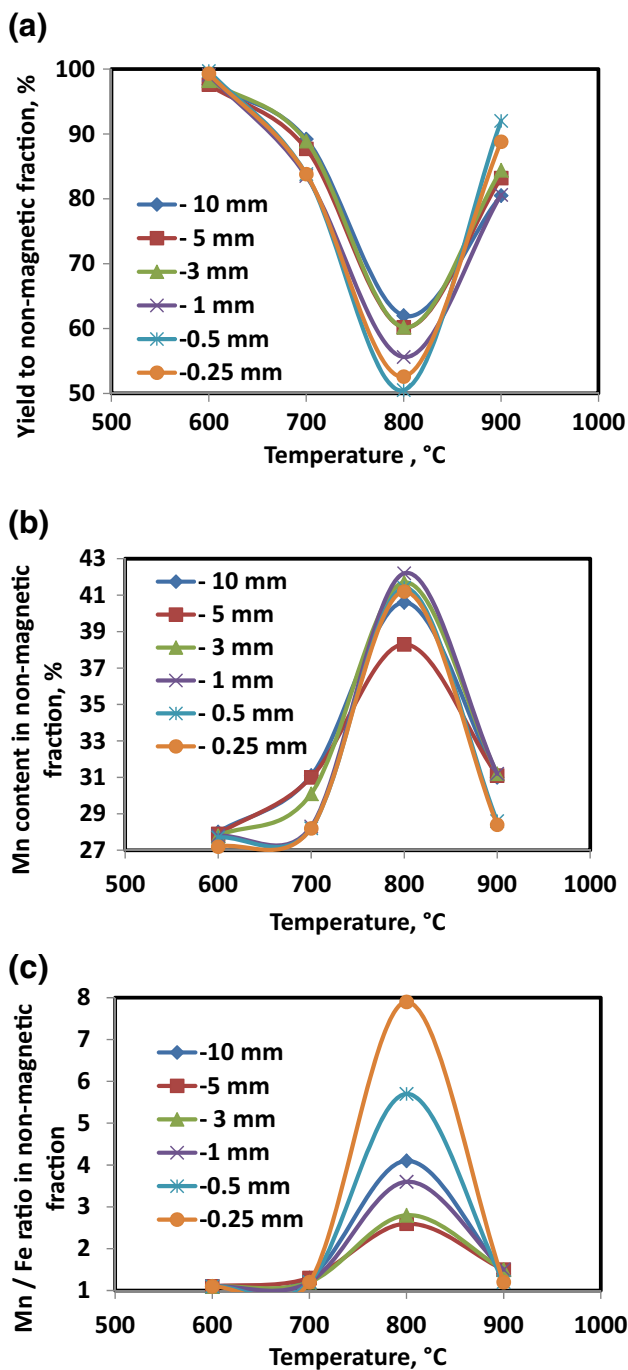


Fig. 3 a Yield, b Mn content, c Mn/Fe ratio of the non-magnetic fraction as a function of particle size and temperature for a fixed time period of 120 min and reductant of 10%

reduction of iron bearing phases in the sample is based on the surface contact with carbon or solid–solid reaction which is efficient at finer particle size. However, from the industrial application point of view, coarser particles are preferred as the permeability of the bed can be maintained properly and moreover, the fines (below 1 mm) cannot be treated as they create accretion over the furnace lining.

Therefore, further studies were carried out with a particle size of – 10 mm.

3.2.2 Effect of Reduction Time

The results of the experiments as discussed above indicate that 800 °C is the preferable temperature where most of the iron oxides get converted to magnetite and report in the magnetic fraction of the LIMS while the manganese oxides report in the non-magnetic product thereby increasing the Mn grade and Mn/Fe ratio. Further experiments were carried out in order to study the effect of the reduction time inside the furnace. The time interval was varied between 30 and 120 min at two levels of temperature i.e. 800 and 850 °C. The particle size of – 10 mm and 10% reductant were kept constant for every experiment.

The results of the experiments as displayed in Fig. 4a indicate that the yield in the non-magnetic fraction, at the temperature of 800 °C, decreases with an increase in the reduction time up to 90 min beyond which it remains almost constant, whereas at temperature 850 °C, time is found to have a minor effect on the yield of non-magnetic fraction as well as Mn content. It is also noteworthy that the yield of the non-magnetic product is lesser at 850 °C when compared to 800 °C. The corresponding higher Mn

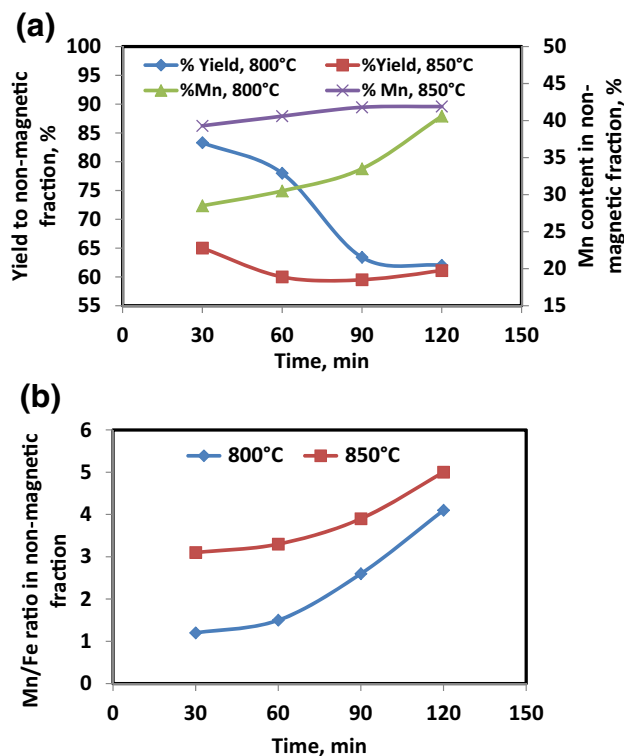


Fig. 4 a Yield and Mn content, b Mn/Fe ratio of the non-magnetic fraction as a function of time for a fixed reductant of 10% and temperature of 800 and 850 °C

grade in case of 850 °C also supports this trend. This may be due to the formation of a higher amount of magnetite content at 850 °C that gets separated in the magnetic fraction of the LIMS resulting in a higher Mn grade and lower yield. However at 800 °C, the reduction to magnetite increases with time and the highest separation of magnetite occurs at a roasting time of 120 min. Therefore, the highest Mn grade of the non-magnetic part is obtained at 120 min. However, the Mn grade at 800 °C is still lower than that for 850 °C. This also explains why the yield of the non-magnetic fraction at reduction temperature at 800 °C is more.

Similarly, the Mn to Fe ratio of the non-magnetic portion is found to be enriched to its maximum at 850 °C (Fig. 4b). It further confirms that the reduction is more effective at the temperature 850 °C as the Mn content of the non-magnetic product is higher than 40%. The results also indicate that optimum products with 60–61% yield and ~ 42% Mn at a Mn/Fe ratio of 4–5 are obtained at the time intervals of 90 and 120 min.

3.2.3 Effect of Reductant

Further attempts were made to understand the effect of reductant amount on the process. Experiments were carried out by varying the reductant dosage in the feed between 6 and 12% at two different time intervals i.e. 90 and 120 min. The other variables such as: – 10 mm particle size and reduction temperature of 850 °C were kept constant. The results of the effect of reductant dosage at two different time periods are given in Fig. 5. From Fig. 5a, it is found that as the time of reduction increases, there is an increase in the yield to the non-magnetic fraction with the increase in the reductant dosage. However, the yield drops down a little with the increase of the reductant content from 10 to 12%. This may be attributed to more magnetite formation due to more surface contact between the reductant and the iron oxide particles. Similarly, the yield at 120 min is higher compared to that at 90 min because of more reduction. It is notable that that the grade of the non-magnetic fraction is ~ 48% when 12% reductant is applied. The Mn to Fe ratios of the non-magnetic fractions are also enriched to ~ 6 with the level of reductant dosage at 12% (Fig. 5b). An almost similar Mn to Fe ratio being observed at 12% reductant for both 90 and 120 min reduction time suggests that time plays a less significant role with this reductant concentration. This also indicates that the kinetics of the reduction of iron oxide is optimum at 90 min for achieving higher Mn to Fe ratio. The overall results suggest that the reductant content should be at least 10% of the burden to reduce the iron bearing minerals effectively. This value also matches with the

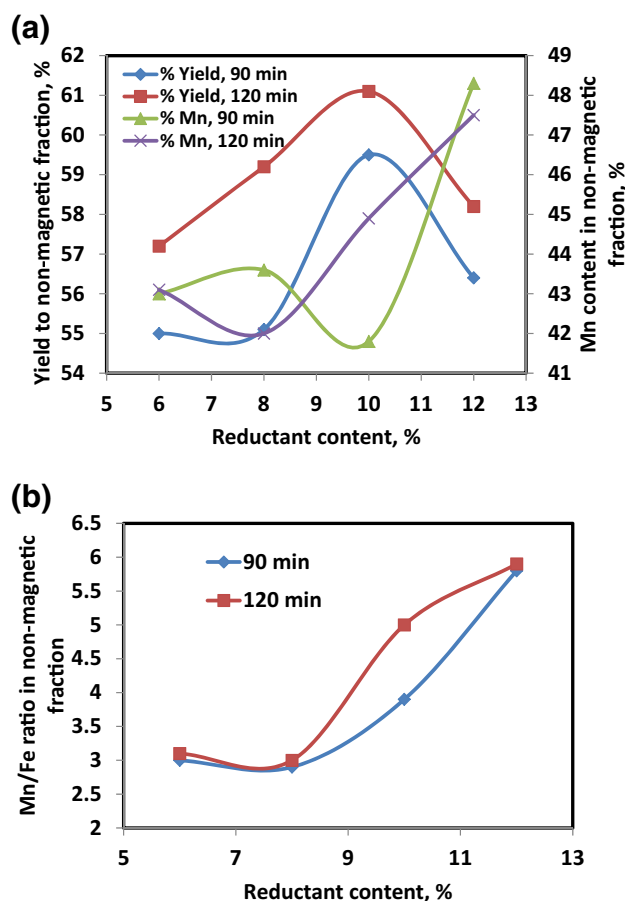


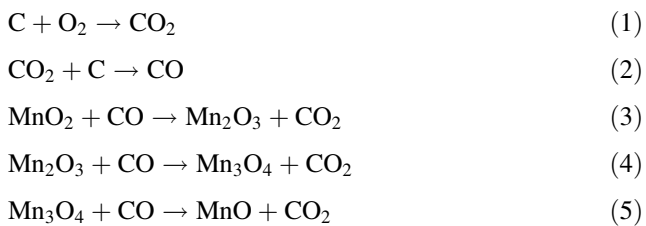
Fig. 5 a Yield and Mn content, b Mn/Fe ratio of the non-magnetic fraction as a function of reductant content at a fixed temperature 850 °C and time periods of 90 and 120 min

required stoichiometric value of the reductant for the reduction of the iron oxide phases to magnetite phases at 850 °C.

The product obtained at a temperature of 850 °C, reductant content of 12% C and roasting time of 90 min contains 48.3% Mn and 8.33% Fe at a yield of 56.4%. The Mn to Fe ratio of 5.8 indicates that it is suitable for the downstream processing towards the making of ferro manganese alloys after suitable treatments.

3.3 Characterization of Roasted Products

The reduction of Mn oxides in the presence of silica and Fe oxides is a complex phenomenon and researchers have reported the formation of carbide phases like $(\text{Fe, Mn})_3\text{C}$ and $(\text{Fe, Mn})_7\text{C}_3$ at temperatures ranging from 1000 to 1300 °C [30, 31]. However, the reduction sequence of manganese oxides, when subjected to reduction either using C or CO follows the below mentioned sequence within a temperature range of 400–600 °C [32, 33].



Iron oxide such as Fe₂O₃ also follows a similar sequence as mentioned in Eqs. 4 and 5. Further, when the temperature rises to around 1000 °C, FeO further reduces to Fe metal. When an iron rich manganese ore is subjected to reduction either using C or CO, it is not thermodynamically feasible to reduce manganese oxides beyond MnO within a temperature of 1000 °C [34]. On the contrary, the iron oxide phases get reduced to Fe₃O₄ and metallic Fe which are strongly magnetic in nature. Therefore, a low intensity magnetic separation unit can separate the reduced iron oxides generating a Mn rich non-

magnetic product. It may also be noted that the formation of Fe₃O₄, in the present work, is at an elevated temperature compared to that required in a pure iron oxide system. This is mainly due to the absence of a proper reducing environment along with the maintained partial pressure during the experimentation. So, the required temperature and kinetics can be further improved by using a suitable reducing atmosphere at different partial pressure. Taking into consideration the above mentioned facts and figures, SEM–EDS studies were undertaken for some of the roasted products so as to understand the formation of different phases and correlate them with the experimental findings.

The overall observation from the back scattered electron images as shown in Fig. 6 suggests the formation of manganite from feed manganese dioxide phases like pyrolusite, cryptomelane and psilomelane as earlier

Fig. 6 SEM BSE images of the roasted products showing, **a** extremely minute sized silicate grains embedded within the Mn oxide phases, formation of manganite after reduction roasting, lithiophorite along the grain boundaries of manganite at the roasting condition of 600 °C and 10% C, **b** development of pores after reduction roasting due to contraction and removal of hydroxides at the roasting condition of 700 °C and 10% C, **c** Lithiophorite along the borders of manganite, **d** bands of manganite and lithiophorite enclosed within silicate gangues, **e**, **f** locked silicates within manganite phases, some silicates have quartz as core and K–Al–Mn silicates as the borders and in some cases there is no border and only K–Al–Mn silicates are present. **c–f** Present the photo micrographs of the samples roasted under the conditions of 850 °C and 12% C

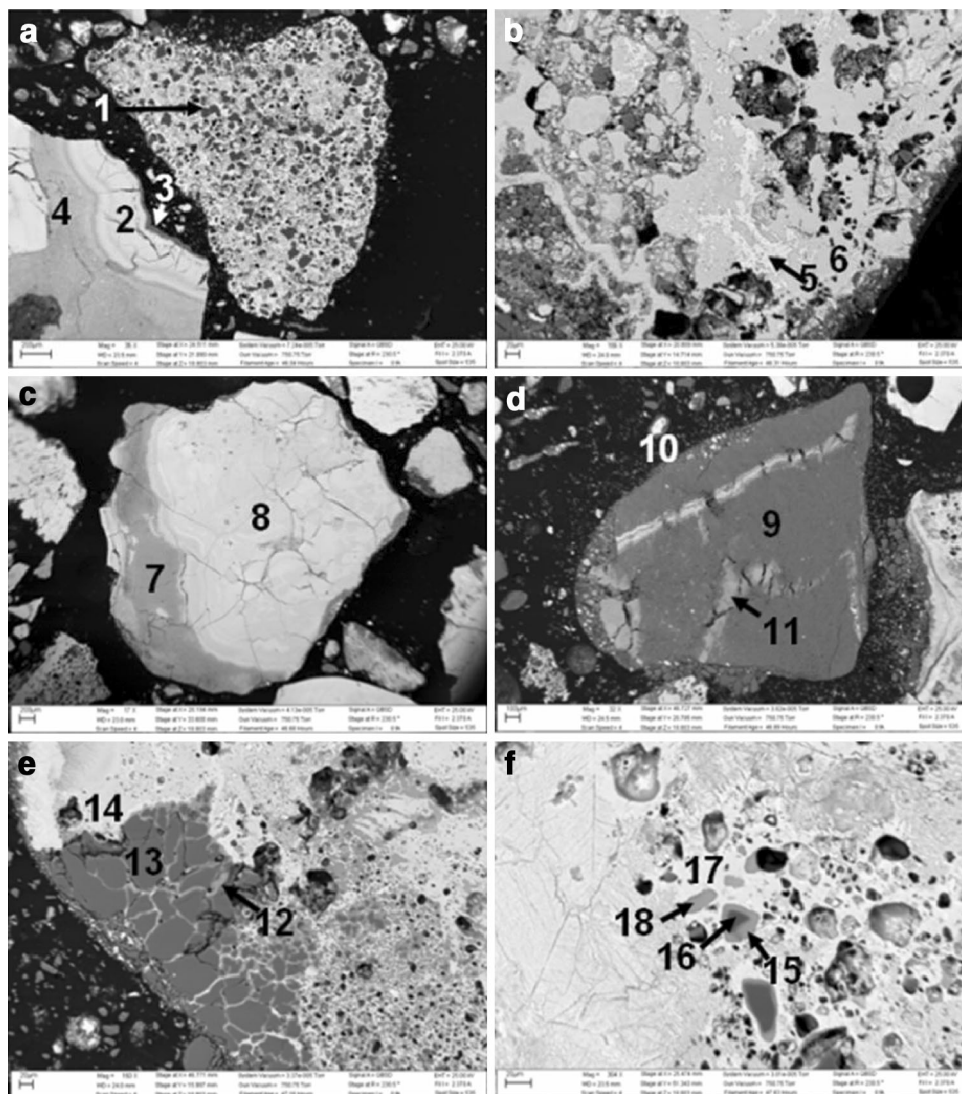


Table 3 SEM–EDS semi-quantitative mineral chemistry of various mineral phases of the roasted products with the numbers 1–18 representing the points marked in the photo micrographs shown in Fig. 6

S. no.	Mineral	O	Mn	Fe	Al	Si	K	Mg	Ti	Ba	Co	Ni	Cu
1	Corundum	51.4	0.64	0.22	46.8	0.45	0.54	0	0	0	0	0	0
2	Manganite	30.5	64.9	0	3.67	0	0	0.1	0.92	0	0	0	0
3	Lithiophorite	42	43.2	2.76	11.1	0.4	0.07	0.51	0	0	0	0	0
4	Manganite	31.7	64.8	0.03	3.06	0.08	0	0.21	0.18	0	0	0	0
5	Jacobsite	31.6	20.1	47.8	0.42	0	0	0.05	0	0	0	0	0
6	Fe–manganite	28.9	58.8	9.81	2.01	0.04	0	0.14	0.23	0	0	0	0
7	Lithiophorite	37.7	40.5	1.38	15.6	2.39	2.16	0	0.04	0	0.2	0	0
8	Manganite	32.7	64.6	1.54	0.55	0	0.48	0.03	0	0	0.1	0	0
9	K–Al–Silicate	53.8	0	1.4	22.4	16.9	5.34	0	0	0.1	0	0	0
10	Manganite	35.9	61.7	0	1.93	0.15	0.07	0.17	0.13	0	0	0	0
11	Lithiophorite	32.7	41.6	3.48	18.5	1.34	0	0.16	0.06	0	0.1	2.2	0
12	K–Al–Mn–silicate	41.2	16.4	0	0.15	28.3	13.9	0	0	0.1	0	0	0
13	Quartz	57	0.51	0.42	0.23	41.6	0.23	0	0	0	0	0	0
14	Manganite	31.3	67.9	0.38	0.27	0	0	0	0	0	0	0.1	0.1
15	K–Al–Mn–silicate	40.7	19.2	0	0.15	22.3	16.8	0	0.19	0	0	0.2	0.5
16	Quartz	57	0.71	0.53	0.16	41.3	0.24	0	0	0	0	0	0
17	Manganite	33.8	59.5	2.95	0.32	2.48	0.96	0.03	0	0	0	0	0
18	K–Al–Mn–silicate	36.3	21.1	0	0.14	21.8	19.6	0	0.09	0	0	0.2	0.6

All the values are given in wt%

reported in Figs. 1 and 2. However, lithiophorite has not changed after reduction roasting (Table 3). Some of the manganite grains formed after reduction roasting are found to be rich in iron. Though the majority of the manganese dioxide phases (pyrolusite, cryptomelane and psilomelane) have converted to manganite, in some other cases, some of the manganese dioxide phases have converted to jacobsonite and iron rich manganite (Table 3). Both manganite and iron rich manganite occur in solid solution states and might have been formed during the roasting by the reaction of Mn and Fe phases at temperature 850 °C with 12% C (Fig. 6 and Table 3). However, quantity wise, the manganite content is more in case of the sample roasted at 850 °C with 12% C (Fig. 6c–f) compared to 600 and 700 °C with 10% C (Fig. 6a, b respectively). The results of the chemical analysis and weight recovery of the magnetic (iron rich phases) and non-magnetic products (Mn rich phases) given in Fig. 4 attest to this fact that the roasting conditions of temperature at 850 °C with 12% C is leading to a better Mn/Fe ratio than the roasting at 600 and 700 °C with 10% C. However under the conditions of temperature: 850 °C and charcoal: 12%, the silicates react with the surrounding cryptomelane giving rise to K–Al–Mn–silicate (Fig. 6e, f and Table 3) which is not observed in the samples roasted at 600 and 700 °C with 10% C. It can be noted that some of the silicate phases have converted completely to K–Al–Mn–silicate while in some other cases, it remains as a rim

around the pre-existing silicate phases like quartz. However, this K–Al–Mn–silicate phase (as indicated by the SEM images; Fig. 6e, f and Table 3) is completely different from the Mn–silicate phase that is present in the head sample. Other than these phases, corundum is also rarely observed in the roasted product (Fig. 6a).

Some iron rich regions in the roasted product obtained under the roasting conditions of temperature: 850 °C and charcoal: 12% were analyzed under the SEM and the results are displayed in Fig. 7 and Table 4. It is observed that the iron phases have mostly converted to magnetite. However, the magnetite formation has been less significant at the temperatures 600 and 700 °C with 10% C. This can be the reason giving rise to a high grade iron concentrate in the magnetic fraction and a Mn rich non-magnetic fraction leading to a better Mn/Fe ratio at the temperature 850 °C.

Mineralogically, if one compares the feed sample with that of the roasted products, then it is clear from the above discussion and pictographic presentation that the manganese dioxide phases like pyrolusite, cryptomelane and psilomelane have converted to manganite in some cases while in other cases, the same have converted to jacobsonite and iron rich manganite. The silicates react with the surrounding manganese dioxide phases particularly cryptomelane giving rise to K–Al–Mn–silicate phase, which is completely different from the Mn–silicate phase that is present in the head sample.

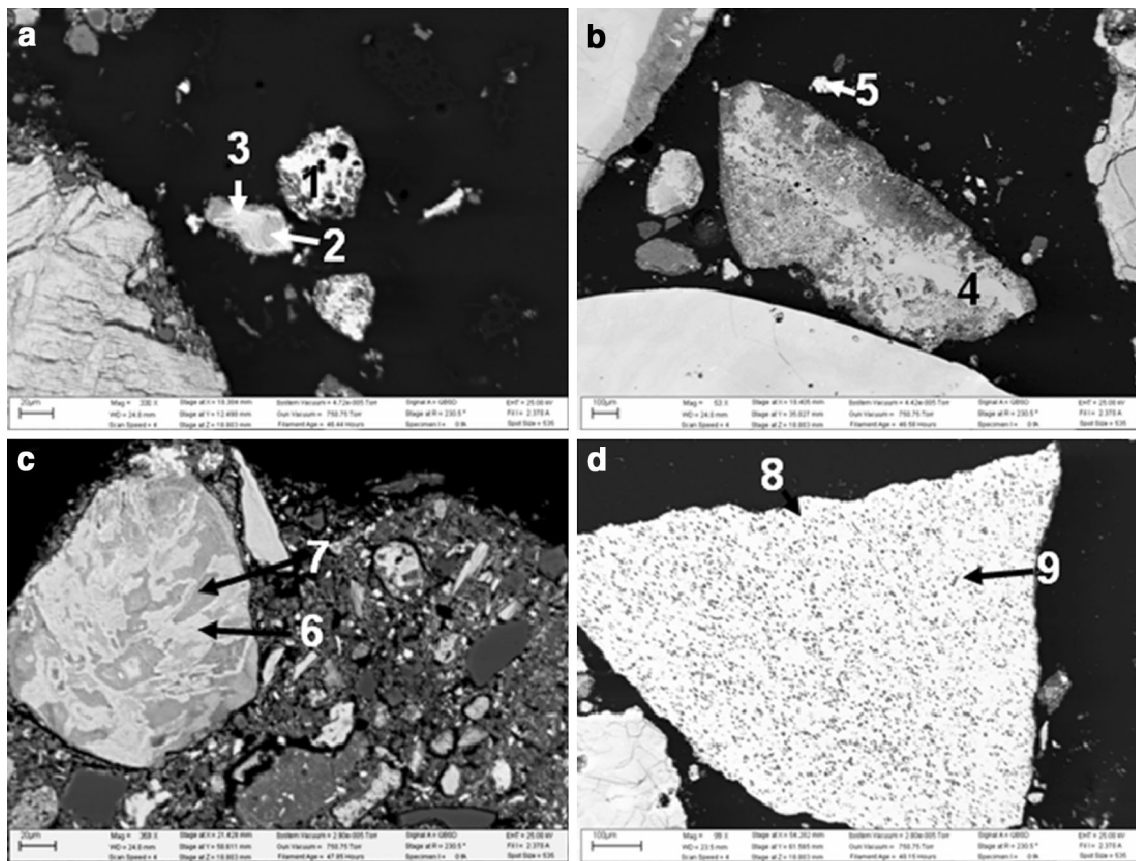


Fig. 7 SEM BSE images of the iron rich region of the roasted products obtained under the conditions of 850 °C and 12% C showing, **a** magnetite and manganite, **b** manganite and hematite in a banded structure, **c** intermingling of manganite and iron rich manganite, **d** magnetite having numerous inclusions of silicates

Table 4 SEM–EDS semi-quantitative mineral chemistry of various mineral phases of the roasted products with the numbers 1–9 representing the points marked in the photo micrographs shown in Fig. 7

S. no.	Elements	O	Mg	Al	Ti	Si	P	Ca	K	Mn	Fe	Co
1	Magnetite	25.8	0.16	0.41	0	0.04	0	0	0	0	73.6	0
2	Manganite	37.6	0.03	4.13	0.01	0.22	0.22	0.11	0	57.7	0	0
3	Manganite	30.3	0.06	1.22	0	0.05	0.05	0.03	0	68.3	0	0
4	Manganite	32.1	0.11	0.68	0	0	0	0	0	67.1	ND	0
5	Hematite	30.3	0.01	0	0	0	0	0	0	ND	67.9	1.82
6	Fe-rich	38.3	0	2	0.13	0.1	0	0.11	0.04	53.4	5.88	0
7	Manganite	32.4	0.04	0.41	0	0	0	0.11	0	67.2		0
8	Magnetite	25.6	0.13	0	0.14	0.06	0	0	0	0	72.3	1.8
9	Fe–Al–K silicate	42.7	ND	14.7	0	11.4	0	0	6.32	0	24.3	0.75

All the values are given in wt%

4 Conclusions

Reduction roasting followed by magnetic separation studies of an iron rich manganese ore were carried out while the pre- and post reduced manganese ore samples were subjected to in-depth characterization studies. The reflected

light microscopic and SEM–EDS studies on the feed sample revealed the presence of different Mn bearing phases like pyrolusite, cryptomelane, psilomelane and lithiophorite along with iron phases such as hematite, goethite and limonite, and many silicate phases. The liberation studies using QEMSCAN established the fact that

the Mn and Fe bearing phases were interlocked in a very complex manner limiting the scope of any physical beneficiation methods for enriching the Mn to Fe ratio to a desired level. The effects of different roasting parameters such as particle size, temperature, reductant percentage and residence time were studied. It was observed that the reduction efficiency was enhanced with fine particle sizes of the ore such as – 500 μm and – 250 μm . However, the conditions of roasting were optimized with a particle size of – 10 mm taking into account the fact that the feasibility of scaling up the process would favour a coarse particle size. The results indicated that under the roasting conditions such as temperature: 800–850 °C, time: 90–120 min and charcoal: 10–12%, it was possible to recover a Mn rich non-magnetic product having 45–48% Mn with a Mn/Fe ratio of 5–6 at a yield of ~ 60% from a feed containing 27.7% Mn and 26.1% Fe. The SEM–EDS semi-quantitative data of the optimum reduced samples proved that manganite was the major Mn phase formed from the phases like pyrolusite, cryptomelane, psilomelane, where as the iron phases were found to be converted to magnetite leading to a better Mn and Fe separation in the low intensity magnetic separation.

Acknowledgements The authors are thankful to the Director, CSIR-IMMT Bhubaneswar for his kind consent to publish this paper and to Tata Steel for funding this research.

References

1. Indian Mineral Year Book, Indian Bureau of Mines, Ministry of steel and mines, Nagpur (2003) p 55.1–55.21.
2. Manganese ore vision 2020 and beyond, Indian Bureau of Mines, Nagpur, India (2014).
3. Xin B, Chen B, Duan N, and Zhou C, *J Bior Tech* **102** (2011) 1683.
4. Mineral Facts & Problems No-4, Monograph on Manganese Ore, Indian Bureau of Mines, Ministry of steel and mines, Nagpur, (1974) p 271–276.
5. Mani K S, and Subrahmanyam D, *Proc Indian Natn Sci Acad*, **50A** (1984) 509.
6. Naik P K, Reddy P S R, and Misra V N, *J Min Metall*, **41A** (2005) 11.
7. Mishra PP, Mohapatra B K., and Mahanta K, *J Miner Mater Charact Eng*, **8** (2009) 47.
8. Sharma T, *Int J Miner Process*, **35** (1992)191.
9. Dash N, Mohapatra B K, and Rao D S, *World Metall. Erzmetall*, **63** (2010) 5.
10. Singh V, Ghosh T K, Ramamurthy Y, and Tathavadkar V, *Int J Miner Process*, **99** (2011) 84.
11. Chanturiya E L, Bashlykova T V, Potkonen N I, and Makavetskas A R, Poor manganese ore dressing on the basis of mineralogical–technological studies, in *Proceedings of the XXI International Mineral Processing Congress*, Rome, **13** (2000) p C2–1.
12. Hosseini M R, Bahrami A, and Pazouki M, Influence of shaking table parameters on manganese grade and recovery, *Proceedings of the XXIV International Mineral Processing Congress (IMPC)*, Beijing, (2008) p 783.
13. Malayoglu U, *Asia J Chem*, **22** (2010) 3292.
14. Tripathy S K, Mallick M K, Singh V, and Murthy Y R, *Powder Technol* **239** (2013) 284.
15. Oliazadeh M, Noaparast M, Dehghan R, Beneficiation of low grade fine manganese ores, *Proceeding of the XXIII International Mineral Processing Congress*, Istanbul (2006) p 347.
16. Singh V, Tathavadkar V, Denys M B, Venugopal R, *Miner Eng*, **32** (2012) 8.
17. Abeidu A M, *Trans JIM*, **14** (1973) 45.
18. Dendyuk T V, *Powder Technol* **71** (1992) 47.
19. Zhou F, Chen T, Yan C, Liang H, *Colloids Surf A Physicochem Eng Asp*, **466** (2015) 1–9.
20. Rao G V, Acharya B C, Murty B V R, Mohanty J N, Swamy Y V, and Tripathy A K, *Magn Electr Sep* **9** (1998a) 109–123.
21. Rao G V, Mohapatra B K, and Tripathy A K, India, *Magn Electr Sep*, **92** (1998b) 69.
22. Kanungo S B, Mishra S K, and Biswal D, *Miner Metall Process*, **17(4)** (2000a) 269.
23. Kanungo S B, Mishra S K, and Biswal D, *Miner Metall Process*, **17** (2000b) 181.
24. Grieco G, Kastrati S, and Pedrotti M, *Miner Process Extr Metall Rev*, **35** (2014) 257.
25. Tripathy S K, Banerjee P K, and Suresh, N., *Int J Miner Metall Mater* **22** (2015) 661.
26. Swamy Y V, Bhoi B, Prakash S, and Ray H S, *Miner Metall Process*, **15** (1998) 34.
27. Kivinen V, Krogerus H, and Daavittila J, Upgradation of Mn:Fe ratio of low grade manganese ore for ferromanganese production, *Proceedings of XII International Ferro Alloys Congress*. Helsinki (2010) p 467.
28. Acharya B C, Rao D S, and Sahoo R K, *Miner Deposit*, **32** (1997) 79–93.
29. Acharya B C, Rao D S, Sahoo R K, and Dash B, *Indian J Geol*, **66** (1994) 15.
30. Kuo K, Persson L E, *J Iron Steel Inst*, **178** (1954) 39.
31. Akdogan G, and Eric R H, *Miner Eng* **7** (1994) 633–645.
32. Ren S J, *Industrial Minerals Resource Exploitation and Processing Handbook*. Wuhan Industry University Press, Wuhan, (1993) p 18–37.
33. Momade F W Y, and Momade Z S G, *Hydrometallurgy* **54** (1999) 25.
34. Gao, Y., *Prereduction and Magnetic Separation of Low Grade Manganese Ore*, M.S. Thesis, University of Utah (2011).